Supplementary Information (SI) for Journal of Analytical Atomic Spectrometry.

Supplementary Information

In-situ measurement of sulfur isotope ratios in sulfide samples with LA-ICP-MS/MS using N_2O and He reaction gas

Estida Eensoo[a*], Päärn Paiste[a], David A. Fike[b], Jennifer L. Houghton[b], Kärt Paiste[a, b],

[a] Department of Geology, University of Tartu, 50411 Tartu, Estonia

[b] Department of Earth & Planetary Sciences, Washington University in St Louis, St Louis, MO 63130, USA

IRMS measurement results of the samples

Table 1. IRMS values of the Uljaste pyrrhotite samples and Zf-pyrite

ID 1	ID 2	$\delta^{34}S$ (‰ VDCT)	Average δ34S (‰ VDCT)	Standard deviation (1 σ)
Uljaste pyrrhotite	227,8	-2,72		
Uljaste pyrrhotite	227,8	-2,35	-2,54	0,27
Uljaste pyrrhotite	265	-4,42		
Uljaste pyrrhotite	265	-3,94	-4,18	0,34
Uljaste pyrrhotite	294,9	-1,61		
Uljaste pyrrhotite	294,9	-1,40	-1,50	0,15
Uljaste pyrrhotite	305,1	-5,98		
Uljaste pyrrhotite	305,1	-6,01	-6,00	0,02
Uljaste pyrrhotite	317	-3,56		
Uljaste pyrrhotite	317	-3,89	-3,72	0,23
Uljaste pyrrhotite	334,5	-5,35		
Uljaste pyrrhotite	334,5	-5,32	-5,34	0,02
Zf Pyrite	outer 1	-11,10		
Zf Pyrite	outer 2	-9,87	-10,48	0,87
Zf Pyrite	inner 1	-11,02		
Zf Pyrite	inner 2	-11,55	-11,29	0,38

Table 2. IRMS values of the Ward's pyrite

Identifier 1	Identifier 2	Reference Value	Calculated value
sulfa	ref		0,73
LCystin	ref		15,83
Atrop	ref		2,00
SO 6	standard	-34,1	-33,99
NBS 127	standard	20,3	20,54
Ward's pyrite	1		-1,33
Ward's pyrite	2		-1,03
Ward's pyrite	3		-1,22
Ward's pyrite	4		-1,04
Ward's pyrite	5		-1,32
SO 6	standard	-34,1	-34,20
NBS 127	standard	20,3	20,06

δ_{VCDT} $\delta^{34}S$ Ward's pyrite: -1.19 ± 0.15

Table 3. IRMS values for Huanzala pyrite

ID1	ID2	$\delta^{34}S$ (‰)	Atm % S	Average δ34S (‰) row
row 1	column 1	2,48	53,36	1,09

row 1	column 2	3,07	55,42	
row 1	column 3	1,34	54,01	
row 1	column 4	0,64	57,47	
row 2	column 1	2,33	56,05	1,13
row 2	column 4	0,72	53,53	
row 3	column 1	2,41	56,24	
row 3	column 2	1,56	55,91	0,66
row 3	column 3	0,84	54,15	
row 3	column 4	1,34	57,14	
row 4	column 1	2,62	56,07	
row 4	column 2	2,64	54,79	0,11
row 4	column 3	2,63	55,05	
row 4	column 4	2,41	51,16	

δ_{VCDT} $\delta^{34}S$
Huanzala pyrite: -1.93 ± 0.82

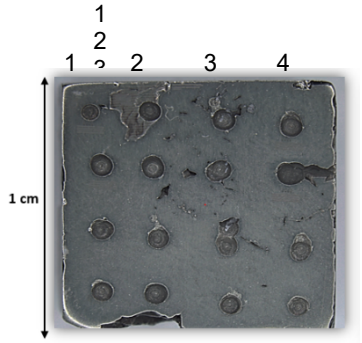

Figure 1. Picture of the Huanzala sample where the drill spots done for IRMS measurement are visible. Row 1 and Column 1 correspond to the outer facet of the cubic crystal

Signal smoothing experiments

Table 4. Signals of different signal-smoothing configurations used to calculate the washout

		SO				SO2			
Interval		Conf A cps	Conf B cps	Conf C cps	Conf D cps	Conf A cps	Conf B cps	Conf C cps	Conf D cps
A	Average 3 s	722290	687958	798337	781266	613075	528833	552535	562904
B	Average 8-10 s	10603	10756	15751	15969	27033	23522	26893	27450
	A/B	68	64	51	49	23	22	21	21
C	Average 78-81 s	10205	10412	13763	13297	26809	23297	25257	25590
	A/C	71	66	58	59	23	23	22	22

Table 5. Washout calculation for different detection modes experiment using configuration D with 7 coils for SO

Interval		P-P spots cps	P-A lines cps	P-A spots natural samples experiment in cps
A	Average 3 s of analysis	735365	31400408	20951525
B	Average 8-10 s	42187	1130834	1084535
	A/B	17.4	27.8	19.3
C	Average from 3 last s	40465	1082188	1061172
	A/C	18.2	29.0	19.7

Reaction gas experiments

Table 6. The efficiency of using only N_2O as the reaction gas and its effects on the main reaction products SO_2 and SO

N2O (%)	10	15	20	25	30	35	40	45	50	60	70	80	90	100
SO2 (cps)	96750	221490	364800	461800	523350	537740	502010	456100	395310	271130	171550	99060	58260	33470
SO (cps)	195780	266130	299660	273320	231940	183710	135610	99680	69930	32490	14600	6210	2830	1370

Table 7. The S reaction products background signals at different 4th gas flow rates (%)

N_2O %	0	20	40	65	80	100
SO^+ (cps)	23	13732	19088	17833	13481	9919
SO_2^+ (cps)	13	5807	20400	49253	71347	84775

Table 8. Reaction efficiency of using N_2O in different concentrations and He in different flow rates for SO_2 expressed in cps

He flow rate (mL/min)	1	1.5	2	2.5	3	3.5	4	5	6	7
N_2O 5%	23030	24790	33480	42700	54210	66340	70730	70480	60440	40630
N_2O 10%	81300	68270	81700	92210	100700	104720	105040	87370	60870	37650
N_2O 15%	100110	107730	110330	116390	116410	107560	97820	73900	43840	23640
N_2O 20%	141880	135750	129580	119590	109480	100220	85300	55640	31730	16320

Table 9. Reaction efficiency of using N_2O in different concentrations and He in different flow rates for SO expressed in cps

He flow rate (ml/min)	1	1.5	2	2.5	3	3.5	4	5	6	7
N_2O 5%	200540	248090	325790	416430	526430	646760	711670	759990	689600	512070
N_2O 10%	350690	371950	458870	526410	594270	624760	647400	573580	419780	267820
N_2O 15%	348820	410110	442190	489110	502750	483160	453990	389150	228220	125340
N_2O 20%	358330	374150	408410	405080	384820	365890	322080	221400	127860	63780

Table 10. Interfering ions, their mass-to-charge ratios (m/z), and relative abundances under optimized analytical conditions for SO and SO_2 product ion formation. The data is collected under "wet" analytical conditions while aspirating ultrapure water into the spray chamber. Q1 was set to m/z 32 and Q2 was scanned from 2-260 m/z. Data is provided as relative signal intensity of the summed signals collected between m/z 2-260. Data has been presented for ions with relative signal intensity >0.01% of the total summed signal

m/z	30	31	32	44	45	46	48	64	88	89	90
Interfering Ion	$^{14}N^{16}O$	$^{14}N^{17}O$, $^{14}N^{16}O^{1}H$	$^{14}N^{18}O$, $^{16}O_2$	$^{14}N_2{}^{16}O$	$^{14}N_2{}^{17}O$, $^{14}N_2{}^{16}O^{1}H$	$^{14}N^{16}O_2$, $^{14}N_2{}^{18}O$, $^{14}N_2{}^{16}OH_2$, $^{14}N_2{}^{17}O^{1}H$	$^{14}N^{16}O^{18}O$, $^{14}N^{17}O_2$, $^{16}O_3$	$^{16}O_4$	$^{14}N_4{}^{16}O_2$	$^{14}N_4{}^{16}O^{17}O$, $^{14}N_4{}^{16}O_2{}^{1}H$	$^{14}N_4{}^{18}O_2$
Relative Abundance at 4.5 mL/min He + 5% N_2O	3.25%	0.01%	92.10%	3.44%	0.90%	0.03%	0.005%	0.001%	0.0002%	0.0001%	0.0000%
Relative Abundance at 35% N_2O	38.88%	0.13%	8.33%	30.40%	18.24%	0.36%	0.01%	0.01%	1.9084%	0.3708%	0.0123%

*As seen from Table 10 the product ion formation rates for 35% N_2O and 4.5 mL/min He + 5% N_2O are markedly different. This showcases that the main reaction pathways for the two optimized reaction gas configurations are different. When only N_2O is used the main product ions are $^{14}N^{16}O$, $^{14}N_2{}^{16}O$, $^{14}N_2{}^{17}O$ or $^{14}N_2{}^{16}O^{1}H$ and $^{14}N_4{}^{16}O_2$. Owing to the relatively high signal at m/z 45 compared to m/z 44, it can be speculated that some H contamination (as H_2O vapor) was present in the used cell gas as the relative ratio between the distribution of signals between m/z 44and 45 can't be attributed solely to ^{16}O and ^{17}O abundances. For 4.5 mL/min He + 5% N_2O reaction gas mixture the main interference is observed on m/z 32 that can mainly be attributed to unreacted $^{16}O_2{}^{+}$ arising from the plasma. The main product ions associated with N_2O are $^{14}N^{16}O$ and $^{14}N_2{}^{16}O$ with similar formation levels. Formation of higher order reaction products as N_4O_2 is negligible.

Effect of detection mode and sample matrix on $\delta^{34}S$ measurements

Table 11. S isotope ratios of pyrite and pyrrhotite samples analyzed in different detection modes and normalized with Ward's pyrite or pyrrhotite

Mode	Normalized with:	Ward's Py (Mean ± Stdev)	Ward's Po (Mean ± Stdev)	ZY-Py (Mean ± Stdev)	Uljaste (Mean ± Stdev)
Pulse-Pulse spots	Pyrite	-0.93 ± 0.35	-0.16 ± 1.88	-10.61 ± 1.56	-1.16 ± 2.67
	Pyrrhotite	-1.26 ± 1.07	-0.10 ± 1.32	-11.72 ± 1.70	-1.33 ± 2.46
Pulse-Analog lines	Pyrite	-1.05 ± 1.03	-0.40 ± 1.57	-9.67 ± 1.51	-1.56 ± 1.86
	Pyrrhotite	1.25 ± 1.49	-0.14 ± 1.65	-7.76 ± 1.75	-1.06 ± 2.14
Pulse-Analog spots	Pyrite	-1.00 ± 1.39	-0.70 ± 1.47	-11.00 ± 1.42	-1.46 ± 1.51
	Pyrrhotite	-0.62 ± 1.04	-0.11 ± 1.62	-9.99 ± 1.30	-1.22 ± 1.19
IRMS control values		-1,188 ± 0.15	-0,11 ± 0.02	-10.49 ± 0.87	-1.51 ± 0.15

Table 12. Bias calculation for different detection modes while normalizing with Ward's Pyrite

Samples	Pulse-Pulse spots	Pulse-Analog lines	Pulse-Analog spots
Ward's Py	0,26	0,14	0,19
Ward's Po	-0,05	-0,29	-0,59
Zf-Py	-0,12	0,82	-0,51
Uljaste	0,35	-0,05	0,05

Table 13. Bias calculation for different detection modes while normalizing with Ward's Pyrrhotite

Samples	Pulse-Pulse spots	Pulse-Analog lines	Pulse-Analog spots
Ward's Py	-0,07	2,44	0,57
Ward's Po	0,01	-0,03	0
Zf-Py	-1,23	2,73	0,5
Uljaste	0,18	0,45	0,29

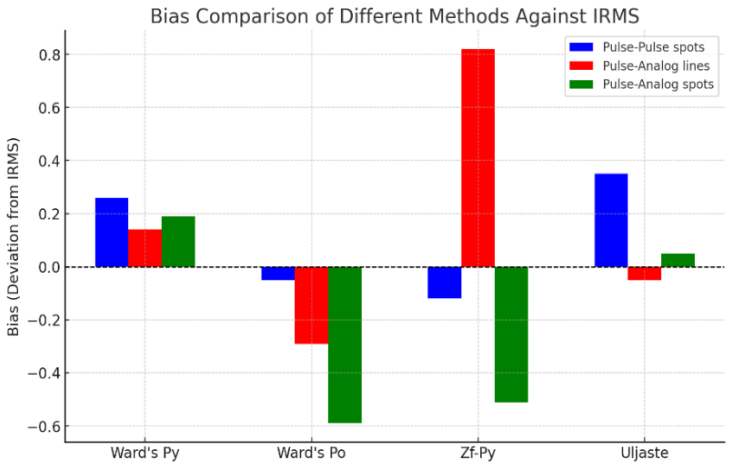

Figure 2. Bias comparison of the samples for different detection modes, while normalizing with Ward's pyrite

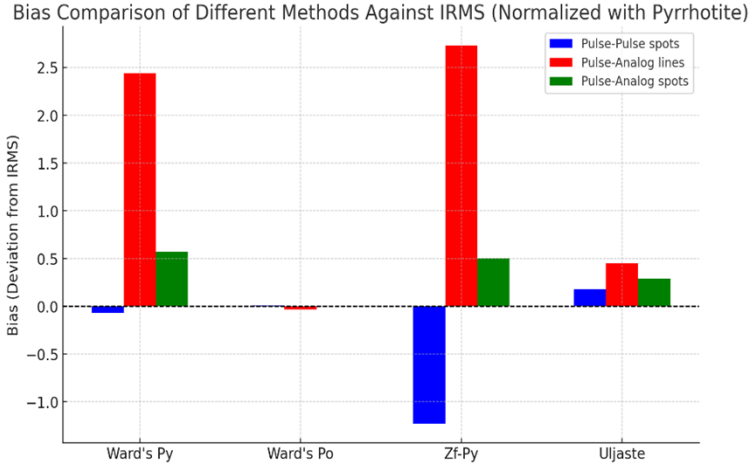

Figure 3. Bias comparison of the samples for different detection modes while normalizing with Ward's pyrrhotite

Measurement of the natural pyrite and pyrrhotite samples

Table 14. S isotope ratios of the natural pyrite and pyrrhotite samples

Sample name	d34 S	Average d34 S	Standard deviation	IRMS value
Uljaste 249 d1	-0.39	-1.60	1.82	-1.51 ±0.148
Uljaste 249 d1 (Copy 1)	-1.68			
Uljaste 249 d1 (Copy 2)	-0.55			
Uljaste 249 d1 (Copy 3)	0.52			
Uljaste 249 d1 (Copy 4)	-0.52			
Uljaste 249 d1 (Copy 5)	-3.99			
Uljaste 249 d2	0.62			
Uljaste 249 d2 (Copy 1)	-4.07			
Uljaste 249 d2 (Copy 2)	-4.20			
Uljaste 249 d2 (Copy 3)	-2.50			
Uljaste 249 d2 (Copy 4)	-0.79			
Uljaste 317	-6.12	-4.35	1.61	-3.73 ±0.23
Uljaste 317 (Copy 1)	-3.99			
Uljaste 317 (Copy 2)	-7.47			
Uljaste 317 (Copy 3)	-3.39			
Uljaste 317 (Copy 4)	-5.32			
Uljaste 317 d2	-3.24			
Uljaste 317 d2 (Copy 1)	-5.19			
Uljaste 317 d2 (Copy 2)	-2.65			

Uljaste 317 d2 (Copy 3)	-2.69			
Uljaste 317 d2 (Copy 4)	-3. 42			
Uljaste 265	-3.17			
Uljaste 265 (Copy 1)	-2.00	-2.76	1.74	-4.18 ± 0.34
Uljaste 265 (Copy 2)	-0.42			
Uljaste 265 d2	-1.87			
Uljaste 265 d2 (Copy 1)	-3.50			
Uljaste 265 d2 (Copy 2)	-5.46			
Uljaste 265 d2 (Copy 3)	-4.32			
Uljaste 265 d2 (Copy 4)	-1.76			
Uljaste 227.8	-2.49	-1.55	1.06	-2.54 ± 0.26
Uljaste 227.8 (Copy 1)	-0.99			
Uljaste 227.8 (Copy 2)	-3.17			
Uljaste 227.8 (Copy 3)	-0.81			
Uljaste 227.8 (Copy 4)	-1.59			
Uljaste 227.8 d2	-2.71			
Uljaste 227.8 d2 (Copy 1)	0.09			
Uljaste 227.8 d2 (Copy 2)	-0.74			
Uljaste 227.8 d2 (Copy 3)	-1.57			
Uljaste 305 d1	-3.48	-5.70	2.36	-6.00 ± 0.02
Uljaste 305 d1 (Copy 1)	-1.01			
Uljaste 305 d1 (Copy 2)	-4.26			

Uljaste 305 d1 (Copy 3)	-8.11			
Uljaste 305 d1 (Copy 4)	-8.65			
Uljaste 305 d1 (Copy 5)	-4.67			
Uljaste305 d2	-5.51			
Uljaste305 d2 (Copy 1)	-4.85			
Uljaste 305 d2 (Copy 2)	-5.09			
Uljaste 305 d2 (Copy 3)	-8.04			
Uljaste 305 d2 (Copy 4)	-8.89			
Uljaste 305 d2 (Copy 5)	-5.81			
Uljaste 334 d1 (Copy 3)	-4.15	-5.19	1.65	-5.34 ± 0.02
Uljaste 334 d1 (Copy 4)	-4.09			
Uljaste 334 d1 (Copy 4)	-7.89			
Uljaste 334 d2	-6.62			
Uljaste 334 d2 (Copy 1)	-4.38			
Uljaste 334 d2 (Copy 2)	-4.02			
Balmat	14.99	15.40	0.98	15.10 ± 0.20
Balmat (Copy 1)	14.29			
Balmat (Copy 2)	14.16			
Balmat (Copy 3)	17.40			
Balmat (Copy 4)	16.07			
Balmat (Copy 5)	15.70			
Balmat (Copy 6)	15.46			
Balmat (Copy 7)	15.47			
Balmat (Copy 8)	15.01			

Zf-pyrite 1	-12.24	-10.28	1.70	-10.49 ± 0.87
Zf-pyrite 2	-11.15			
Zf-pyrite 3	-12.48			
Zf-pyrite 4	-9.63			
Zf-pyrite 5	-8.12			
Zf-pyrite 6	-9.53			
Zf-pyrite 7	-8.78			

Table 15. Bias values for natural sulfide samples

Sulfide samples	Bias
Uljaste 227.8 (n=9)	0,98
Uljaste 249 (n=11)	-0,09
Uljaste 265 (n=8)	1,45
Uljaste 305 (n=12)	0,30
Uljaste 317 (n=10)	-0,62
Uljaste 334 (n=6)	0,15
ZF pyrite (n=7)	0.21
Balmat 1 (n=9)	0,78

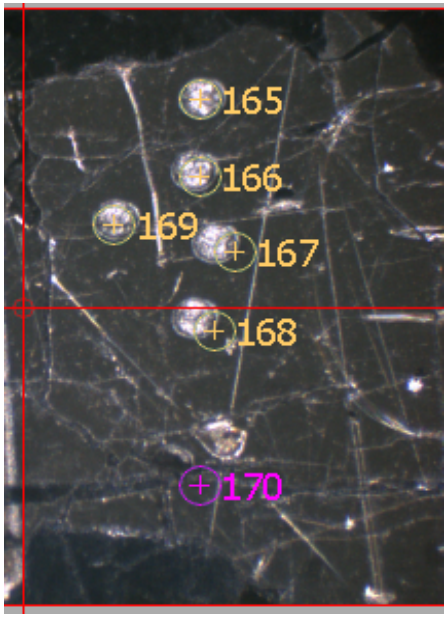

Figure 4. Image of ablation spots on sulfide sample. Due to laser shift, the actual ablation spots are slightly misaligned, and the ablation in spot 170 occurred on a cracked surface. This spot and others placed on cracked surfaces or not entirely located on the sulfide matrix were discarded from further data reduction based on visual inspection.